

Unraveling of quantum effects in bosonic Josephson junctions: a dynamical multi-configuration atomic coherent states approach

Yulong Qiao and Frank Grossmann

Institut für Theoretische Physik, Technische Universität Dresden, D-01062 Dresden, Germany

(Dated: February 13, 2023)

The mean-field approach to two-site Bose-Hubbard systems is well established and leads to non-linear classical equations of motion for the population imbalance and the phase difference. It can, e.g., be based on the representation of the solution of the time-dependent Schrödinger equation either by a single Glauber state or, for finite systems, by a single atomic (SU(2)) generalized coherent state [S. Wimberger et al., Phys. Rev. A **103**, 023326 (2021)]. We demonstrate that quantum effects beyond mean field are easily uncovered if, instead, a multi-configuration ansatz with a few time-dependent SU(2) basis functions is used in the variational principle. For the case of plasma oscillations, the use of just two time-dependent basis states can already give good qualitative agreement of the phase space dynamics with numerically exact quantum solutions. In order to correctly account for more non-trivial dynamics, like spontaneous symmetry breaking as well as macroscopic quantum self trapping, more basis states are needed.

I. INTRODUCTION

The Bose-Hubbard (BH) model of S interacting (bosonic) atoms in optical lattices is the basis of many state of the art experimental [1–4] as well as theoretical efforts [3, 5]. The cold atom Hubbard tool box introduced in the latter reference puts a focus on strongly interacting many-body dynamics and embraces the fields of quantum optics, quantum computation and solid state physics. The BH model is a paradigm for the rich physical phenomena exhibited in these areas, such as there are quantum phase transitions between the superfluid and the Mott insulator phase [1] and self-trapping in bosonic Josephson junctions [6], to name just a few.

Restricting the amount of lattice sites makes the quantum dynamics of the BH model easily tractable numerically for moderate particle numbers. Recent theoretical work has thus focused on the cases of four (and six) sites [7] with different levels of approximation: exact, semiclassical and classical (mean-field, or truncated Wigner approximation (TWA)). Also the trimer (ring) case has been studied, due to the facts that it is leading to the melting of discrete vortices via quantum fluctuations [8] and that it is the smallest system that displays chaotic mean-field dynamics without an external driving term [9]. This system has also been dealt with using a group theoretical [10, 11] and a semiclassical time-domain approach [12]. With an additional drive (periodic kicks) even the double well case is showing signatures of chaos [13]. Furthermore, the case of two wells without external driving has been extensively studied. The system dynamics has, e.g., been investigated both in a mean-field classical approximation and fully quantum mechanically [6, 14–16], as well as also semiclassically, using a phase space picture [17] or employing the Herman-Kluk propagator [12, 18, 19]. This same propagator has also been used in a semiclassical time-domain study of the single well problem [20]. Furthermore, the driven single well problem has served as a model in a study of dynamical tunneling [21].

An important lesson from the vast literature is that semiclassical approaches do well in reproducing the full quantum results, while the mean-field and/or truncated Wigner approach have their limitations. TWA does, e.g., not allow for the investigation of revival phenomena, present in the quantum dynamics. The most surprising phenomenon, that could already be uncovered using a mean-field approach based on the Gross-Pitaevskii equation, is the macroscopic quantum self trapping effect in bosonic Josephson junctions, where the population imbalance (to be defined below) has a nonzero average [6]. It turns out that mean-field theory predicts the transition to macroscopic quantum self trapping at too large values of the on-site interaction strength, however [22].

In the following, we will focus on the case of two wells, for which the direct experimental observation of tunneling and self trapping has become possible [23]. Theoretically, this case has been reviewed in [24] and a fresh look on finite size (i.e., finite particle number) effects in a mean-field description of those Josephson junction systems has been given by Wimberger et al. [22]. These authors have used a so-called atomic or SU(2) generalized coherent state [25], to uncover mean-field $1/S$ corrections to the more familiar mean-field results based on standard Glauber coherent states. We will also employ those favorable number conserving SU(2) states here. We will not use them in a mean-field spirit, however, where just a single state is taken to solve the time-dependent Schrödinger equation (TDSE). In contrast, we will investigate what happens if we allow for non-trivial multiplicity, which for reasons of simplicity we first choose to be just two, i.e., we will use a superposition of two SU(2) states to solve the TDSE. From previous experience with semiclassical Gaussian-based approaches to solve the TDSE for molecular Hamiltonians [26, 27], as well as for the spin boson problem [28, 29], we are confident that only a handful of suitable time-dependent basis states could be enough to achieve satisfactory agreement with exact quantum solutions if a full fledged variational approach is taken. In order to correctly account for more demanding quan-

tum effects like self trapping, it will turn out that the multiplicity has to be increased, but it can still be kept below the total number of time-independent Fock states that has to be used in a full quantum calculation.

The presentation is structured as follows: In order to set the stage, in Sec. 2 we will review the variational approach, based on a single atomic coherent state (ACS), to the mean-field solution of the bosonic Josephson junction. At the end of this section, a special focus will be put on the stability analysis of the nonlinear classical phase space dynamics. In Sec. 3, we then choose an ansatz wave-function with non-trivial multiplicity, employing a small number of time-evolving atomic coherent states to represent the quantum beat dynamics of the BH dimer. In a brief review of the quantum phase operator concept, we establish the relation between the phase difference in mean field and its quantum analog. This allows us to compare numerical results for phase space trajectories with the corresponding solution of the TDSE. We will cover a broad range of system parameters as well as initial conditions. It will turn out that there are cases, close to the equilibrium point of the classical dynamics, in which just two ACS will suffice to achieve reasonable agreement with exact results. For large initial population imbalance/phase difference as well as for large (as well as attractive) on-site interaction strength, the number of ACS will have to be increased, however. In the last section we give conclusions and an outlook on possible future work. Supplementary material can be found in two appendices.

II. TWO-SITE BH MODEL AND MEAN FIELD DYNAMICS

A. The Hamiltonian

The simplest Hamiltonian for the bosonic Josephson junction (two-site BH model) in normal ordered form reads

$$\hat{H} = -J(\hat{a}_1^\dagger \hat{a}_2 + \hat{a}_2^\dagger \hat{a}_1) + \frac{U}{2} \sum_{j=1}^2 \hat{a}_j^{\dagger 2} \hat{a}_j^2, \quad (1)$$

where the bosonic ladder operators \hat{a}_j and \hat{a}_j^\dagger with commutation relation $[\hat{a}_j, \hat{a}_j^\dagger] = \hat{1}$ destroy, respectively create a particle (a bosonic atom) in the site labelled by the index j . Furthermore,

$$\hat{n}_j = \hat{a}_j^\dagger \hat{a}_j, \quad j = 1, 2 \quad (2)$$

counts the number of particles per site and $\hat{S} = \hat{n}_1 + \hat{n}_2$ is the total number operator and its expectation value S is a conserved quantity, because \hat{S} commutes with \hat{H} . The site expectations n_1, n_2 may take on any value larger or equal to zero, as long as the constraint $n_1 + n_2 = S$ is fulfilled.

The (dimensionless) parameters U and $J > 0$ denote the strength of the on-site interaction, determined by the s-wave scattering length of the atomic species considered, and the tunneling amplitude, respectively. Later on, we will consider positive and negative values of U , corresponding to repulsive and attractive interaction between the atoms, respectively.

B. Mean-field dynamics

The evolution of the BH model is governed by the time-dependent Schrödinger equation (TDSE)

$$i|\dot{\Psi}(t)\rangle = \hat{H}|\Psi(t)\rangle \quad (3)$$

for the wave-function $|\Psi(t)\rangle$. Here as well as in the remainder of this paper we have set $\hbar = 1$. In order to solve for the dynamics, in the present section we will be following closely the mean-field work presented in [22]. Firstly, we recall the eigenvalue equation of the annihilation operator in the form

$$\hat{a}_j |\alpha_j(t)\rangle = \alpha_j(t) |\alpha_j(t)\rangle = \sqrt{n_j(t)} e^{i\phi_j(t)} |\alpha_j(t)\rangle, \quad (4)$$

with the time-dependent Glauber coherent state

$$|\alpha_j(t)\rangle = e^{-|\alpha_j(t)|^2} e^{\alpha_j(t)\hat{a}^\dagger} |0\rangle \quad (5)$$

and time-dependent site average particle number $n_j(t)$ and phase $\phi_j(t)$.

The approximate mean-field dynamics can then either be obtained by using an Ansatz in terms of a direct product of Glauber coherent states or, instead, by choosing generalized SU(2) coherent states (or atomic coherent states (ACS) [25]), defined by

$$|\Psi(t)\rangle = \frac{1}{\sqrt{S!}} \left(\sqrt{\frac{1+z(t)}{2}} \hat{a}_1^\dagger + \sqrt{\frac{1-z(t)}{2}} e^{-i\phi(t)} \hat{a}_2^\dagger \right)^S |0,0\rangle \\ = |S, \sqrt{\frac{1+z(t)}{2}}, \sqrt{\frac{1-z(t)}{2}} e^{-i\phi(t)}\rangle. \quad (6)$$

Here $|0,0\rangle$ is a shorthand notation for the direct product of two single-particle vacuum states and the time-dependent parameters

$$z(t) = \frac{n_1(t) - n_2(t)}{S} \quad (7)$$

and

$$\phi(t) = \phi_1(t) - \phi_2(t) \quad (8)$$

are the (normalized) population imbalance and the relative phase of the two sites, respectively [22]. The time-dependent particle number expectations at site j can take on fractional values. As a simple example, the reader may want to consider the case of $S = 2$ and initial $z(0) = 1/2$, for which $n_1(0) = 3/2$ and $n_2(0) = 1/2$.

If the system dynamics is governed by a harmonic oscillator Hamiltonian or a Rabi model (single harmonic mode coupled to a spin system), the use of standard so-called Glauber coherent states is common [30, 31]. In the present case, we opt for using generalized coherent states (GCS) [32, 33] instead of Glauber coherent states, however. This is because the former are better suited to describe particle number conserving dynamics, as the latter consist of a superposition of number states in the general case [34, 35]. For Bose-Einstein condensates (BEC) this observation has also been made by Schachenmayer et al. [36], who call the ansatz for a condensate wavefunction with Glauber coherent states the “naive” ansatz and show that it is only equivalent to the GCS ansatz in the case of large particle numbers $S \rightarrow \infty$. Furthermore, it is worthwhile to note that the GCS is the ground state of the “free-boson” model, i. e., the BH model with vanishing on-site interaction, $U = 0$ [6, 37, 38].

The representation of the GCS in the last line in Eq. (6) is motivated by the general expression of a multimode generalized coherent state (total number of modes given by M) in the form [39]

$$|S, \vec{\xi}\rangle = \frac{1}{\sqrt{S!}} \left(\sum_{i=1}^M \xi_i a_i^\dagger \right)^S |0, 0, \dots, 0\rangle, \quad (9)$$

with complex parameters $\{\xi_i\}$, which obey the “normalization” condition $\sum_i |\xi_i|^2 = 1$. The representation of the unit operator in these states has been used in [40] to establish an exact variational dynamics of the multimode Bose-Hubbard model. The number of independent real parameters of the GCS in the two-site case, $M = 2$, is three (two complex numbers minus the normalization condition mentioned above) but there is an overall phase factor that is irrelevant, however, so that we just remain with the two real parameters z and ϕ introduced above. In the case of arbitrary site numbers, the equations for the ξ parameters are referred to as discrete nonlinear Schrödinger equation, which can be viewed as the discrete analog of the Gross-Pitaevskii equation for a BEC [41].

In the following, we will focus on the Josephson junction case and will review the derivation of the equations of motion for the real parameters $z(t)$ and $\phi(t)$, however. To this end, as in [40] and analogous to the procedure in [22], the time-dependent variational principle (TDVP) [42] can be used. The corresponding Lagrangian (time arguments suppressed) is given by

$$L := i\langle \Psi | \partial_t | \Psi \rangle - \langle \Psi | \hat{H} | \Psi \rangle = S \frac{1-z}{2} \dot{\phi} + JS \sqrt{1-z^2} \cos \phi - \frac{U}{4} S(S-1) z^2. \quad (10)$$

The Hamiltonian matrix element appearing there also arises from the mean field Gross-Pitaevskii formalism [43], however, without the $1/S$ correction term appearing in the summand proportional to $S(S-1) = S^2(1-1/S)$. In a last step we now subtract $S\dot{\phi}/2$ from L because

adding a total time-derivative to the Lagrangian will not change the equations of motion of the parameters, as had already been noticed in the PhD work of Göppert-Mayer [44] (see also Exercise 3.4 in [45]), thus yielding

$$\tilde{L} = -\frac{S}{2} z \dot{\phi} + JS \sqrt{1-z^2} \cos \phi - \frac{U}{4} S(S-1) z^2. \quad (11)$$

From the Euler-Lagrange equations

$$\frac{\partial \tilde{L}}{\partial \alpha} - \frac{d}{dt} \frac{\partial \tilde{L}}{\partial \dot{\alpha}} = 0, \quad (12)$$

with $\alpha \in \{z, \phi\}$ we obtain

$$\dot{z} = 2J \sqrt{1-z^2} \sin \phi := f_1, \quad (13)$$

$$\dot{\phi} = -2J \frac{z}{\sqrt{1-z^2}} \cos \phi - U(S-1)z := f_2, \quad (14)$$

which are equations of motion of non-rigid pendulum type [46]. A stationary solution of the above coupled nonlinear equations is given by the equilibrium points $(0, 2\pi n)$ with $n = 0, \pm 1, \pm 2, \dots$

In the next step, we linearize the system of equations around one of the equilibrium points. The Jacobian matrix [47] at $(z^*, \phi^*) = (0, 0)$ is

$$\mathbf{J} = \begin{pmatrix} \frac{\partial f_1}{\partial z} \Big|_{z^*, \phi^*} & \frac{\partial f_1}{\partial \phi} \Big|_{z^*, \phi^*} \\ \frac{\partial f_2}{\partial z} \Big|_{z^*, \phi^*} & \frac{\partial f_2}{\partial \phi} \Big|_{z^*, \phi^*} \end{pmatrix} = \begin{pmatrix} 0 & 2J \\ -2J - (S-1)U & 0 \end{pmatrix} \quad (15)$$

and its eigenvalues are

$$\lambda_{\pm} = \pm \sqrt{2J} \sqrt{-2 + \frac{U}{J} - \frac{US}{J}}. \quad (16)$$

The so-called strength parameter

$$\Lambda = U(S-1)/(2J) \quad (17)$$

is an appropriate parameter combination to be used frequently in the following. More details on the linearized mean-field equations around the phase space origin can be found in Appendix A.

A qualitative change in the mean field dynamics will occur, when the radicant in Eq. (19) changes sign, which happens at the critical value $\Lambda_{SSB} = -1$, where the index SSB stands for spontaneous symmetry breaking [37]. If $\Lambda > -1$, both eigenvalues are imaginary, which indicates that the above equilibrium point is a stable one and the solution is symmetric around the origin, whereas $\Lambda < -1$ will lead to the emergence of another class of stable equilibrium points. The symmetry breaking solutions are located around the stationary point(s) $(z^{SSB}, \phi^{SSB}) = (\pm \sqrt{1 - \frac{1}{\Lambda^2}}, 2\pi n)$ of the system of equations (13,14), where $n \in \mathbb{Z}$ [22]. The corresponding Jacobi matrix is

$$\mathbf{J} = \begin{pmatrix} 0 & \frac{2J}{\sqrt{\Lambda^2}} \\ -2J\Lambda(1 + \Lambda\sqrt{\Lambda^2}) & 0 \end{pmatrix} \quad (18)$$

and its eigenvalues are

$$\lambda_{\pm} = \pm \frac{2J\sqrt{-\Lambda^4 - \Lambda\sqrt{\Lambda^2}}}{\sqrt{\Lambda^2}}. \quad (19)$$

If $\Lambda < -1$ these are imaginary and the solution of the linearized equations around the SSB points are oscillatory.

A further conclusion that can be drawn from the full mean-field equations (13,14) is the fact that the quantity

$$E = \frac{US}{4}(S-1)z^2 - JS\sqrt{1-z^2}\cos\phi \quad (20)$$

is a constant of motion [22]. This leads to the existence of a parameter regime, in which the imbalance cannot become zero during an oscillation cycle and therefore, the average value of z will be nonzero. The condition for this macroscopic quantum self trapping (MQST) effect is $E(z(0), \phi(0)) > E(0, \pi) = JS$. In terms of the strength parameter introduced above, the onset of self trapping is at [48]

$$\Lambda_{\text{MQST}} = \frac{1 + \sqrt{1 - z^2(0)} \cos\phi(0)}{z^2(0)/2}. \quad (21)$$

In contrast to the case of spontaneous symmetry breaking, the MQST effect sets in at large positive values of U (repulsive interaction).

C. Numerical example

As an instructive example, we take $J = 1$ and $S = 20$ for the tunneling parameter and the total particle number, and use the initial condition $(z(0), \phi(0)) = (0.1, 0)$. The critical value of U/J for SSB is $-\frac{2}{19} \approx -0.105$ and in Fig. 1 we draw some mean field trajectories in the phase space spanned by z and $\sin(\phi)$ for different values of U , which we take to be both positive (repulsive interaction) as well as negative (attractive interaction). We choose to display $\sin(\phi)$ on the y -axis, instead of the usual ϕ , in order to ease comparison with the full quantum results to be presented below.

For decreasing values of U , that are still larger than the critical SSB value, ellipsoidal oscillations with decreasing amplitude along the y axis are observed. For the small values of z and ϕ that we consider, these plasma oscillations with frequency $\Omega := 2J\sqrt{1 + \Lambda}$ [49] can be derived analytically, as shown in Appendix A. The solution given there in the case $\Lambda > -1$ explains the independence of the amplitude of the oscillation in z on the on-site interaction, as well as the decrease of the oscillation amplitude of ϕ by the decrease of U .

The trajectory in the case $U = -0.11J$ (green curve), for which $\Lambda = -1.045$, is much different from the other cases, however. Also for this type of solution analytical considerations can be made, if z and $|\phi|$ are still small, as shown in Appendix A. The full mean-field solution, instead of oscillating in an ellipsoidal fashion around the

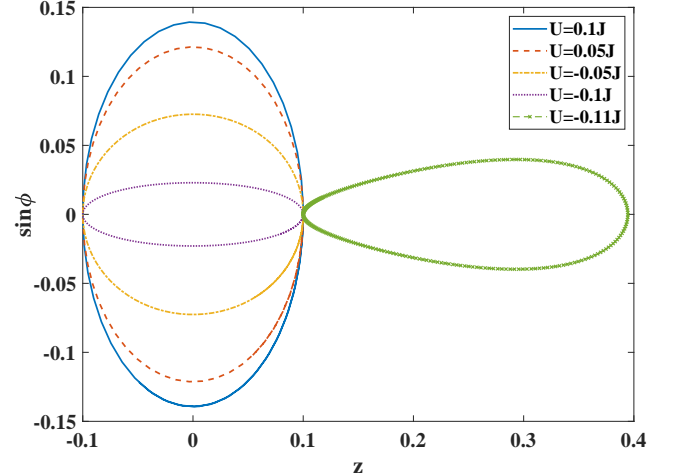


FIG. 1: Phase space trajectories from the mean-field dynamics for different values of on-site interaction strength: $U = 0.1J$ (solid blue), $U = 0.05J$ (dashed red), $U = -0.05J$ (dash-dotted yellow), $U = -0.1J$ (dotted purple), $U = -0.11J$ (green stars). The initial condition for all cases is $(z, \phi) = (0.1, 0)$ and $S = 20$.

For the smallest value of U , dynamical symmetry breaking of z is observed.

stable fixed point at the origin, displays a population imbalance that increases and then decreases again, performing a plectrum-shaped orbit around $(z_{\text{SSB}}, \phi_{\text{SSB}}) = (0.29, 0)$. This breaking of the symmetry of $z(t)$, i. e., the fact that the population imbalance does not oscillate around zero in the mean-field solution was alluded to above. The purple curve (for which $U = -0.1J$) indicates that just before the SSB regime, the eccentricity of the ellipse is strongly enhanced.

Mean-field results for conditions close to MQST will be given in the next section, together with the exact quantum results and results which are gained by employing more than just a single ACS.

III. BEYOND MEAN FIELD DYNAMICS

Due to the shortcomings of the mean-field approach for $U \neq 0$, as there are the absence of collapses and revivals of the population imbalance [14], as well as failures in the prediction of the onset of MQST [22], we will now go beyond mean field by employing a multi-configuration ansatz for the solution of the TDSE.

As a step towards exactness of the solution, we replace the wave-function of Eq. (6) by a linear combination of N time-dependent SU(2) coherent states, written as in the general SU(M) case of Eq. (9), leading to

$$|\Psi(t)\rangle = \sum_{k=1}^N A_k(t) |S, \xi_{k1}(t), \xi_{k2}(t)\rangle. \quad (22)$$

We stress that all the parameters, compactly written as vectors \mathbf{A} (with N entries) and ξ (with $2N$ entries), are time-dependent and complex-valued. Their (nonlinear) equations of motion, again derived from the TDVP, in the general case of arbitrary multiplicity N as well as site number M have been given in matrix form in the appendix of [40]. In addition, this also allows to use the numerical tricks that have been devised in [50] for the case of Glauber coherent state basis functions, if necessary. Because of the restriction to $M = 2$ of the site number in the present investigation, at least for moderate particle numbers, the TDSE can also be solved easily by an expansion of the wave-function in (time-independent) Fock states, whose coefficients fulfill a system of coupled linear first order differential equations. The number of Fock states that are required is determined by the particle number via $S + 1$. More details on the full quantum (Fock space) calculations, whose results will be referred to as exact quantum results in the following, are given in Appendix B.

From the wave-function, we can calculate the populations by taking expectation values of the operators from (2) and from this the imbalance z between the two sites. For the analog of the relative phase ϕ , we use the quantum phase operator concept [8, 51], leading to the expectation values

$$\langle \cos \hat{\phi} \rangle = \frac{\langle \hat{a}_2^\dagger \hat{a}_1 + \hat{a}_2 \hat{a}_1^\dagger \rangle}{\sqrt{2 \langle 2\hat{n}_1 \hat{n}_2 + \hat{n}_1 + \hat{n}_2 \rangle}} \quad (23)$$

$$\langle \sin \hat{\phi} \rangle = \frac{i \langle \hat{a}_1^\dagger a_2 - a_2^\dagger a_1 \rangle}{\sqrt{2 \langle 2\hat{n}_1 \hat{n}_2 + \hat{n}_1 + \hat{n}_2 \rangle}} \quad (24)$$

$$\langle \sin^2 \hat{\phi} \rangle = \frac{1}{2} - \frac{\langle (\hat{a}_2^\dagger \hat{a}_1)^2 + (\hat{a}_2 \hat{a}_1^\dagger)^2 \rangle}{2 \langle 2\hat{n}_1 \hat{n}_2 + \hat{n}_1 + \hat{n}_2 \rangle} \quad (25)$$

of the cosine and sine of the phase operator and its sine square. In addition, the variance of the sine is defined by

$$\Delta(\sin \hat{\phi}) := \langle \sin^2 \hat{\phi} \rangle - \langle \sin \hat{\phi} \rangle^2. \quad (26)$$

The normalization condition $\langle \sin^2 \hat{\phi} + \cos^2 \hat{\phi} \rangle = 1$ and the expectation of $\cos^2 \hat{\phi}$ from [8] have been used to derive Eq. (25).

The relation between the sine of the classical phase variable, displayed in Fig. 1 and the expectation of the sine of the quantum phase is

$$\langle \sin \hat{\phi} \rangle = \frac{S\sqrt{1-z^2}}{\sqrt{S(S-1)(1-z^2) + 2S}} \sin \phi, \quad (27)$$

as can be derived by applying the operator in (24) to an ACS. For $S \rightarrow \infty$, the prefactor on the RHS of the above equation becomes unity and the quantum and classical expressions become identical. Furthermore, in [8] it has been shown that the melting of coherence between the two sites is mirrored by the vanishing of the expectation of $\cos \hat{\phi}$ and the occurrence of large fluctuations of the corresponding variance.

In the following, we will focus on parameters on the border as well as inside of the most interesting regime, the so-called Josephson regime, for which the parameters fulfill the condition $1 < US/(2J) \ll S^2$ [24]. Depending on the initial conditions, beyond mean-field effects can be observed in this case. In addition, we will also allow for negative values of the strength parameter Λ smaller than -1, in order to study the SSB case and will employ large positive Λ values close to the (mean-field) MQST regime.

A. Plasma oscillations

In the following, we first consider the case of small on-site interaction. In addition, also the initial imbalance shall first be small. In a second step, this imbalance shall be large at $t = 0$.

1. Small initial population imbalance

For small values of U , as well as of z , we only include two ACS in the Ansatz in Eq. (22), i. e., we use $N = 2$. Initially, ξ can be still be parameterized in analogy to the procedure of the previous section by $(\xi_{11}, \xi_{12}) = (\sqrt{\frac{1+z_1}{2}}, \sqrt{\frac{1-z_1}{2}} e^{-i\phi_1})$ and $(\xi_{21}, \xi_{22}) = (\sqrt{\frac{1+z_2}{2}}, \sqrt{\frac{1-z_2}{2}} e^{-i\phi_2})$. To highlight the changes that the inclusion of an additional basis state leads to, for the first SU(2) state, we use three different initial conditions, namely $z_{1,i} \in \{0.01, 0.05, 0.1\}$, $\phi_1 = 0$, $A_1 = 1$. For the second SU(2) state, the initial values are identical and are fixed as $z_2 = 0$, $\phi_2 = 2\pi/3$, $A_2 = 0$.

The phase space trajectories in three different levels of approximation and for the three different initial conditions specified above are shown in Fig. 2, for $S = 20$ and an on-site interaction strength of $U = 0.1J$, implying $US/(2J) = 1$. We stress that the expectation value of the sine of the phase operator is plotted on the y -axis. Its relation to the sine of the phase difference in the mean-field case is given in Eq. (27).

In mean-field approximation all three initial conditions give rise to an ellipsoidal pattern as shown in the previous section. Going beyond mean field by allowing for just one additional SU(2), we see a qualitatively different behaviour which corresponds to a beating of the population imbalance, here displayed by a spiraling motion that first moves inward and then outward for all three initial conditions. This is shown not to be an artefact by comparison to the full quantum solution, which shows an almost quantitative agreement with the multiplicity 2 ACS solution. We stress that the choice of the initial phase of the second ACS is decisive for the quality of our beyond mean-field results. Choosing ϕ_2 to be zero, e.g., would lead to a spiraling in the wrong direction.

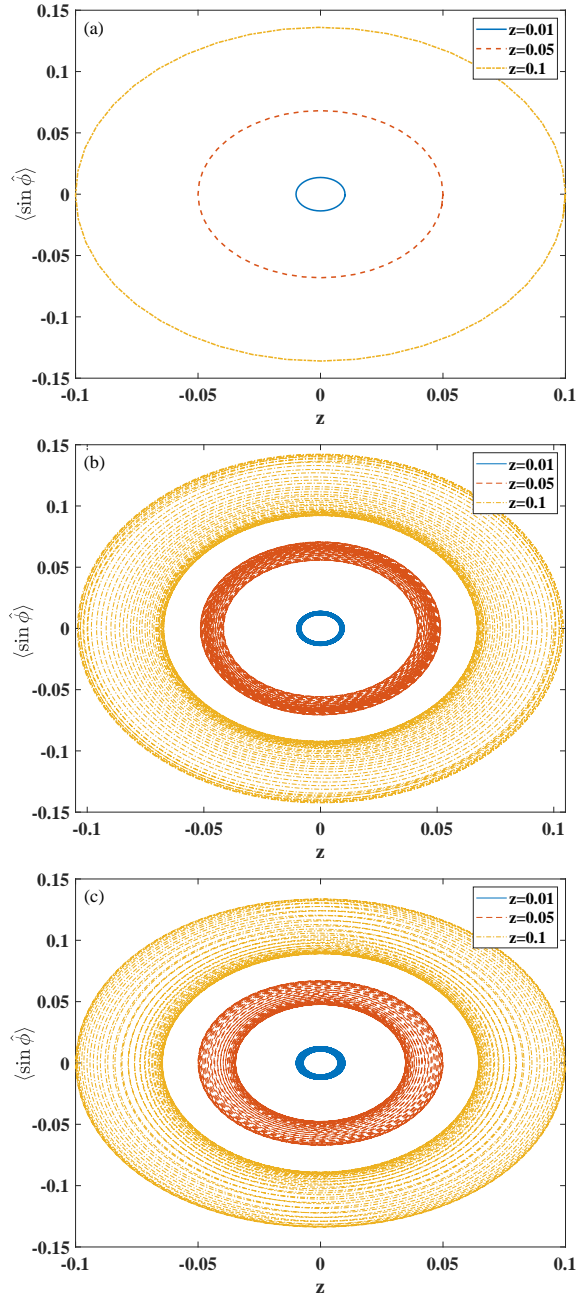


FIG. 2: Phase space trajectories in: (a) mean-field, (b) beyond mean field using ACS with $N = 2$, and (c) exact quantum dynamics. Different initial conditions are indicated by different line styles: $z = 0.01$ (solid blue), $z = 0.05$ (dashed red), $z = 0.1$ (dash-dotted yellow). System parameters are $U/J = 0.1$ and $S = 20$.

2. Large initial population imbalance

The small initial imbalance in the previous case has led to an incomplete collapse, i.e., the oscillation amplitude was still rather large in all three cases at all times, with only small beating amplitude. In order to suppress the

total oscillation amplitude, i.e., to see very small oscillations at least temporarily, we have to allow for larger initial imbalances, which will be done next. For the case of $U = 0.1J$ and with $z_1 = 0.5$, the exact quantum dynamics for two different total particle numbers, $S = 20$ and $S = 50$, is shown in Fig. 3. Corresponding mean-field calculations (not shown) would display a closed oscillation without any spiraling in (decrease of the oscillation amplitude). In the quantum case, however, we see an almost complete collapse of the amplitude, the larger the particle number. For the larger S , in addition, the population imbalance as well as the expectation of the sine of the phase operator stay around zero for a longer time (see also Fig. 4).

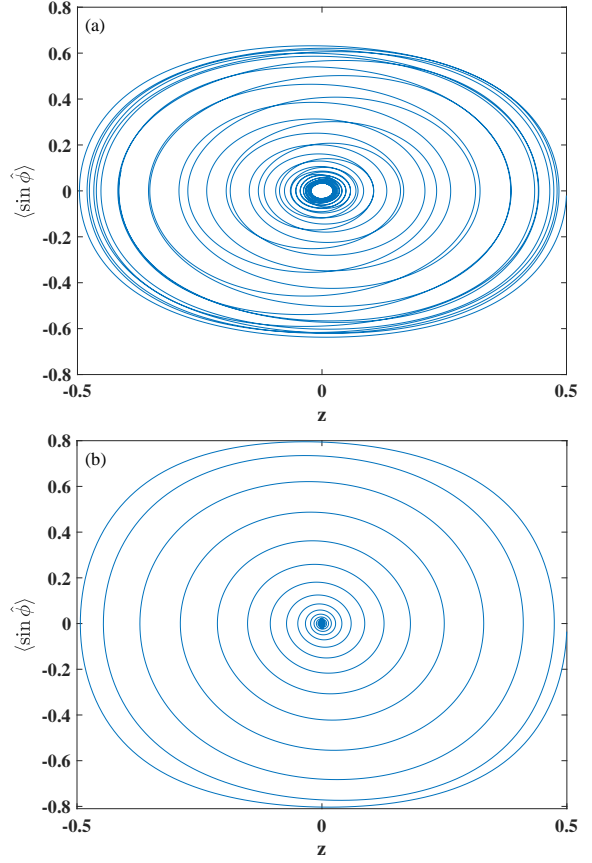


FIG. 3: Exact quantal phase space trajectories for times up to $Jt = 100$ in the case $U/J = 0.1$ for (a) $S = 20$ and (b) $S = 50$. The initial condition is $z_1 = 0.5$ in both cases.

In Fig. 4 we display the time evolution of the sine of the phase operator and its variance as defined above. The results of the beyond mean-field approach and exact quantum calculations are compared. First, we observe the collapse and revival in the case of $S = 20$. For $S = 50$, the maximum time considered is too short to observe the revival, however. Also we can see that the suppression of the oscillation amplitude of $\langle \sin \hat{\phi} \rangle$ comes along with an increase in the amplitude of variance oscillation.

Furthermore, agreement almost within line thickness between exact and ACS results can be achieved, but only if the multiplicity is increased considerably compared to the previous case of small initial imbalance. The multiplicities needed are $N = 8$ in the case of $S = 20$ and $N = 20$ in the case of $S = 50$. The occurrence of large amplitude oscillations in the variance has to be accounted for by an increase in the multiplicity, because in the single ACS case the relative phase is well-defined. We note that both multiplicities are smaller than the total number of Fock states required, which is $S + 1$. Furthermore, the choice of the initial conditions for the initially unpopulated ACS is done in the random fashion explained in detail in [40].

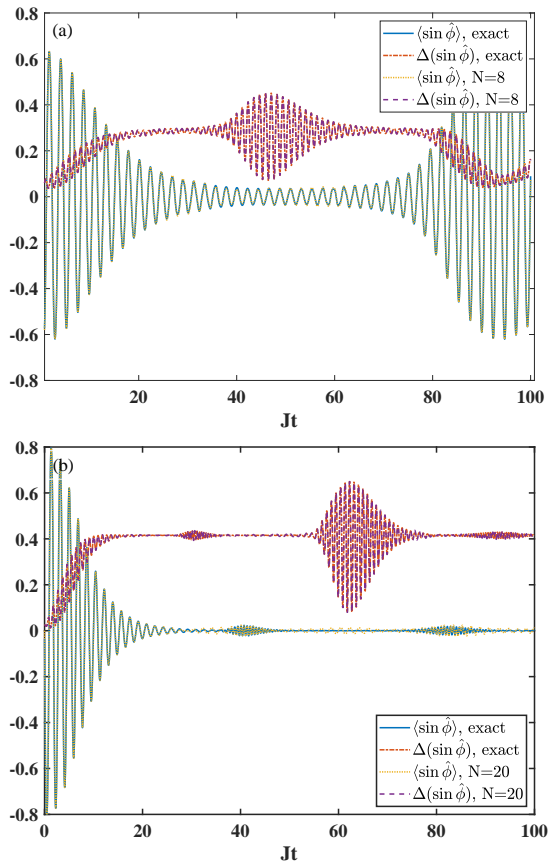


FIG. 4: A comparison of beyond mean-field and exact quantum results for (a) $S = 20$ and (b) $S = 50$. The initial condition is $z_1 = 0.5$ in both cases. The system parameter is $U/J = 0.1$. The expectation value of the sine of the phase (exact results: solid blue line, multi ACS results: dotted yellow line) and its variance (exact results: dash-dotted red line, multi ACS results: dashed purple line) are displayed.

B. Spontaneous symmetry breaking

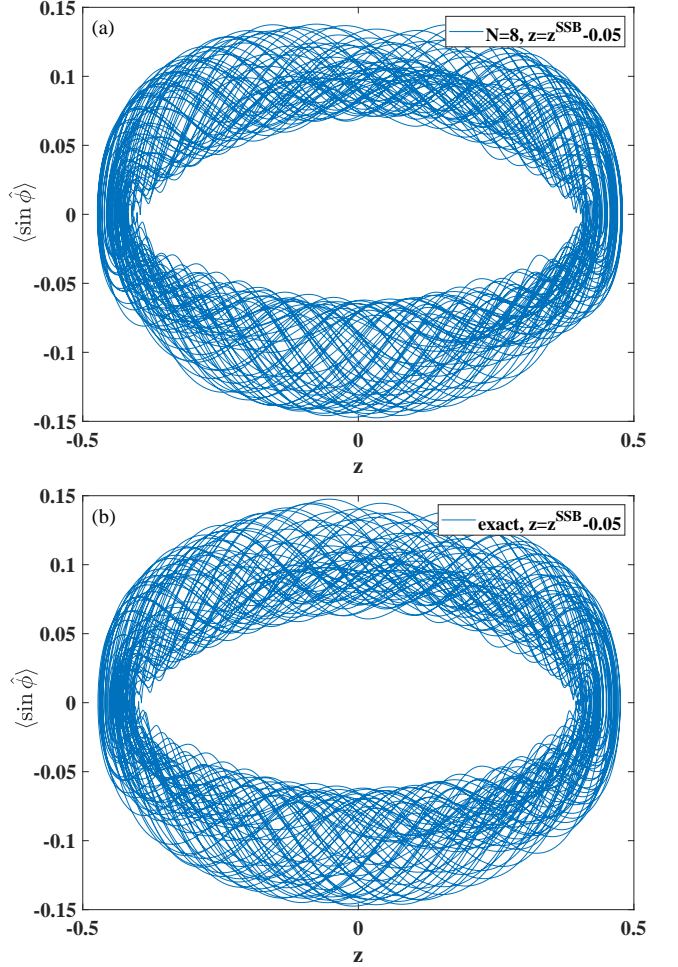
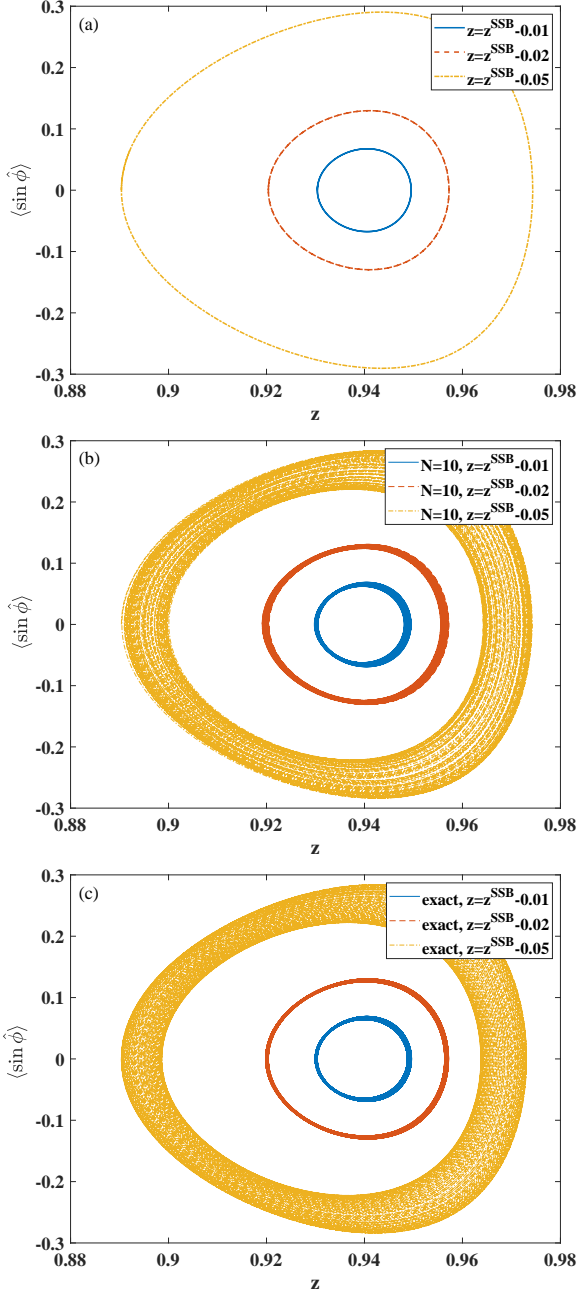
So far, we have focused on positive on-site interaction strength. It was already observed on the mean-field level, however, that a spontaneous symmetry breaking is triggered by negative values of U beyond a certain threshold. The full quantum solution as well as our ACS approach to this case will be in the focus of the present section, where we take $U = -0.12$, leading to $\Lambda < -1$ for $S = 20$, as well as for $S = 50$.

In Fig. 5 we first consider the case of large particle number $S = 50$. Results of three different levels of approximation are again displayed: mean-field, ACS with small multiplicity (here $N = 10$) and full quantum. In the mean-field case, displayed in panel (a), we observe that the elliptic orbit for small deviations from the symmetry breaking equilibrium point ($z^{\text{SSB}} \approx 0.94, \phi^{\text{SSB}} = 0$), for larger displacements turns into the plectrum shaped orbit that is displayed as the green curve in Fig. 1. As in the previous section, multi-configuration ACS with a small multiplicity of $N = 10$ displays the spiraling away from the mean-field orbit (the “quantum effect”) in very faithful way. The further away from z^{SSB} the initial condition is, the broader the range of the spiraling motion turns out to be.

The case of smaller particle numbers $S = 20$ leads to $z^{\text{SSB}} \approx 0.48$ and the phase space trajectories in the beyond mean-field and exact quantum case show a much different behavior than in the mean-field case. We have evolved the trajectories for very long times (up to $Jt = 1000$) in order to almost completely cover the allowed part of phase space. By doing so, in Fig. 6, it can then be observed that the allowed region is very different from the mean-field prediction and the full quantum motion shows no trace of symmetry breaking any more! This behaviour is confirmed by the in-depth study of SSB in [37]. There it was shown that the SSB effect comes along with the switch from a unimodal to a bimodal distribution of the amplitudes in a Fock space expansion of the ground state of the Hamiltonian. For smaller particle numbers, the onset of this effect, compared to the mean field prediction, is pushed to larger absolute values of U (i. e., stronger attractive interaction), as shown nicely in Fig. 4 of [22]. Using just a handful of ACS, we can thus unravel this quantum effect dynamically, without having to calculate the exact ground state.

C. Macroscopic quantum self trapping

In order to see self trapping in the Josephson regime by the restriction of the dynamics to positive values of z (at least for finite times), the initial condition and/or the on-site interaction strength has to be changed. From a mean-field argument the condition given in Eq. 21 has been derived, which is valid at all times. In the following, we will use $z(0) = 0.5$ and $\phi(0) = 0$. This leads to $\Lambda_{\text{MQST}} \approx 15$. We are choosing the total number of



we take $U/J = 0.53$, leading to $\Lambda \approx 14.4$ and $\Lambda \approx 13.0$, respectively. Both values are deep inside the Josephson regime.

In Fig. 7, the results for the phase space trajectories followed up to a total time of $T = 50J$ are displayed. As dictated by our choice of parameters, the mean-field results do not display the MQST effect just yet. The quantum MQST has set in already, however. The fact that in the exact quantum results MQST happens for smaller coupling strengths than in mean field has also been reported in [22]. There it was found that the use of a single ACS does not allow one to observe this quantum effect (the reduction of the critical Λ value), however. By consulting the red curves in Fig. 7, it can be seen that in order for the ACS-ansatz to show the correct quantum behavior (early onset of MQST) a non-trivial multiplicity has to be employed. In our present case this is $N = 12$ for the case $S = 20$ and $N = 25$ for the case $S = 50$. The

particles and the on-site interaction strength such that the actual value of Λ is just below the critical mean-field one, and that the classical dynamics therefore will not be trapped but the strength parameter is large enough for the quantum trajectory to be trapped at positive values of z [22]. For $S = 20$, we take $U/J = 1.2$ and for $S = 50$,

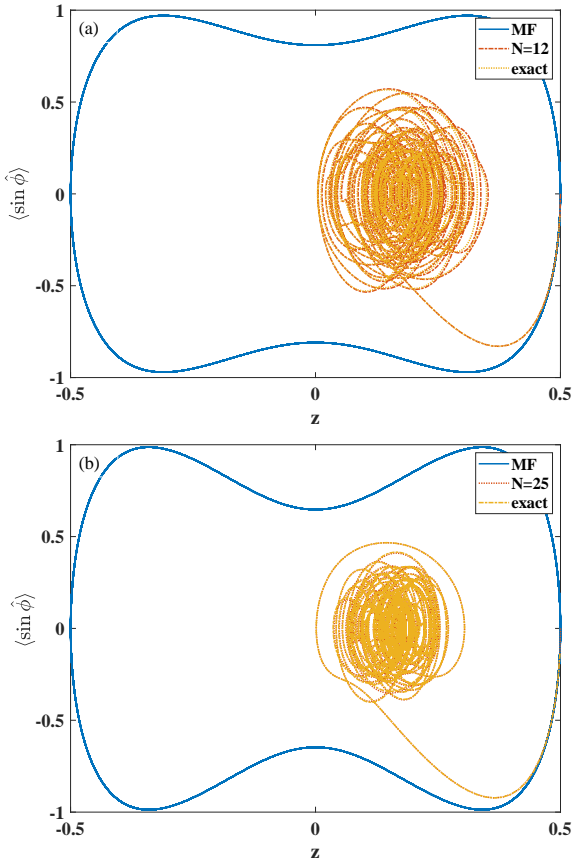


FIG. 7: Phase space trajectories for times up to $Jt = 50$ in mean field approximation (solid blue) multi ACS (dash-dotted red) and exact quantum dynamics (dotted yellow). The initial condition is $(z(0), \langle \hat{\phi}(0) \rangle) = (0.5, 0)$. System parameters are: (a) $U/J = 1.2$ and $S = 20$ and (b) $U/J = 0.53$ and $S = 50$.

high multiplicities needed are due to the fact that both the initial condition in z and also U are rather large. A single ACS will only give the exact quantum solution for $U = 0$, however.

IV. CONCLUSIONS AND OUTLOOK

We have reinvestigated some well-known physical phenomena in the dynamics of the bosonic Josephson junction model. It was shown that, by use of an expansion of the wave-function in multiple ACS, a bridge can be built between classical mean-field results, which are founded on the use of a single ACS (or SU(2) generalized coherent state), and full quantum results. Whereas in a Fock space calculation, the full basis has always to be used, in the present approach, the size of the time-dependent basis can be increased in order to achieve convergence and to unravel quantum effects. The equations of motion for the (time-dependent) variational parameters as well as for the expansion coefficients are derived from

the time-dependent variational principle. This technical aspect of the presented work is similar in spirit to the variational solution of the Gross-Pitaevskii equation with long range interactions, based on Gaussian wavepackets (Glauber coherent states) [52] as well as to the multi-configurational time-dependent Hartree-Fock method for bosons [53], although in the latter case, the employed basis functions are orthogonal.

The parameter space that we have covered is characterized by the strength (and the sign) of the on-site interaction as well as by the total particle number and the initial population imbalance. Firstly, by taking into account one additional ACS, i. e., by employing a total of just two ACS, the beating of the population imbalance (as well as of the expectation of the sine of the phase operator) for small positive values of U can be reproduced almost quantitatively exactly, if the initial imbalance is rather small, i. e., if it is close to the classical equilibrium point at the origin of phase space. The choice of the initial phase variable of the second ACS was crucial to achieve this agreement. For larger initial imbalance, the number of ACS needed to achieve reasonable agreement with the exact quantum results has to be increased, with more and more states needed, the higher the total particle number.

Secondly, for large negative values of the on-site interaction and for large particle numbers, we observed a beating oscillation around the symmetry breaking equilibrium point, that still resembles the mean-field trajectory, with the only quantum effect being the spiraling in and out of the phase space trajectory. For small particle numbers, compared to the mean-field prediction, the symmetry breaking only occurs for larger attractive interaction in the quantum case, however [22]. The fact that the symmetry breaking is lost for parameters that would allow for symmetry breaking in mean-field theory is uncovered by using just ten ACS.

Lastly, our focus was on the most demanding parameter regime of MQST. There, we could show that the use of more than ten ACS is necessary, if the quantum reduction compared to the mean-field value of the repulsive interaction strength at which MQST sets in is to be uncovered. As had been noticed before by Wimberger et al. [22], a single ACS is not enough to observe this effect. In the case of higher multiplicities $N > 2$, the choice of initial conditions for those ACS that are initially unpopulated (i., e., the ones, whose coefficients A_k in Eq. (22) are zero) was done by the random sampling described in [40].

In future works, the fact that the addition of only a few generalized coherent state basis functions allows for the unraveling of quantum effects can be put to good use. A possible extension of the present work would be keeping the site number at two but allowing for more than just a single atomic species [54]. Furthermore, driven bosonic Josephson junctions show dynamical tunneling [55] and the addition of a decay term in one of the sites allows for a characteristic modulation of the self-trapping

[56]. The description of these effects beyond mean field is a worthwhile topic of future investigations. Finally, if one also lets the site number M grow, it might be the only possibility to use flexible time-dependent GCS basis functions if numerical results showing quantum effects are asked for. This is due to the fact that the number of Fock state basis functions grows like $\frac{(M+S-1)!}{S!(M-1)!}$ and Fock state calculations become unfeasible.

Acknowledgments

The authors would like to thank Prof. A. R. Kolovsky for computer code to perform the exact (Fock space) calculations, whose results were displayed here.

Appendix A: Linearized mean-field equations and their solution

From the Jacobi matrix in Eq. (18) we read off the linearized equations of motion

$$\dot{z} = 2J\phi, \quad (A1)$$

$$\dot{\phi} = -[2J + U(S-1)]z \quad (A2)$$

for the population imbalance and the phase difference, valid around the phase space origin. Employing the initial conditions $z(0) = z_0, \phi(0) = 0$, their solution is given by

$$z(t) = \frac{z_0}{2} \left[e^{2J\sqrt{-(1+\Lambda)}t} + e^{-2J\sqrt{-(1+\Lambda)}t} \right], \quad (A3)$$

$$\phi(t) = \frac{z_0}{2} \sqrt{-(1+\Lambda)} \left[e^{2J\sqrt{-(1+\Lambda)}t} - e^{-2J\sqrt{-(1+\Lambda)}t} \right], \quad (A4)$$

with the strength parameter Λ , defined in Eq. (17) of the main text.

If $\Lambda > -1$, we have the oscillatory solutions

$$z(t) = z_0 \cos(\Omega t) \quad (A5)$$

$$\phi(t) = -z_0 \sqrt{1+\Lambda} \sin(\Omega t) \quad (A6)$$

with the plasma frequency

$$\Omega = 2J\sqrt{1+\Lambda}. \quad (A7)$$

We stress that for the specific choice of initial condition, the oscillation amplitude of ϕ depends on the strength parameter, while that of z does not (see also Fig. 1).

If $\Lambda < -1$, we obtain

$$z(t) = z_0 \cosh \left[2J\sqrt{-(1+\Lambda)}t \right], \quad (A8)$$

$$\phi(t) = z_0 \sqrt{-(1+\Lambda)} \sinh \left[2J\sqrt{-(1+\Lambda)}t \right], \quad (A9)$$

which describes the green solution in Fig. 1 at the tip of the plectrum, where the conditions $|z|, |\phi| \ll 1$ are still fulfilled. Away from that regime the hyperbolic solution is unphysical.

Appendix B: Exact quantum calculation

For the exact quantum results, we employ an expansion of the wave-function in terms of Fock states

$$|\Psi(t)\rangle = \sum_{i=0}^S b_i(t) |F_i\rangle, \quad (B1)$$

where the sum is taken over all the states $\{|F_i\rangle\}$ that emerge if a total of S particles is distributed over two sites. It is immediately obvious that there are $S+1$ different possibilities.

In order to completely specify the problem, the initial state has to be known, from which the b coefficients at $t = 0$ can be extracted. In the present work, we consider an initial state that is given in terms of a single ACS with parameters ξ_1 and ξ_2 . From the definition given in Eq. (9) taken for $M = 2$, by applying the binomial theorem, due to $(\hat{a}_i^\dagger)^n |0\rangle = \sqrt{n!} |n\rangle$, we find

$$\begin{aligned} |\Psi(0)\rangle &= \frac{1}{\sqrt{S!}} (\xi_1 \hat{a}_1^\dagger + \xi_2 \hat{a}_2^\dagger)^S |0, 0\rangle \\ &= \sum_{j=0}^S \sqrt{\frac{S!}{(S-j)!j!}} \xi_1^{S-j} \xi_2^j |S-j, j\rangle, \end{aligned} \quad (B2)$$

which is the Fock state expansion of the initial state, providing us with the sought for coefficients at $t = 0$.

One option to evolve the wave-function over time would be to solve the coupled system of linear differential equations for the b coefficients

$$i\dot{b}_j(t) = \sum_{i=0}^S \langle F_j | \hat{H} | F_i \rangle b_i(t), \quad (B3)$$

that follows from the TDSE, e. g., by using a Runge-Kutta method or by matrix exponentiation (which in the present case of time-independent Hamiltonian turns out to be advantageous, because the matrix exponential has to be calculated only once, before the propagation loop is started). An alternative, also numerically exact approach would require diagonalising the BH Hamiltonian in the Fock basis. The time evolution is then finally given by ($\hbar = 1$)

$$|\Psi(t)\rangle = \sum_{i=0}^S c_i \exp\{-iE_i t\} |\Phi_i\rangle, \quad (B4)$$

where the E_i are the eigenenergies and the $|\Phi_i\rangle$ are the eigenstates. The time-independent c coefficients follow from the expansion of the initial wave-function in the eigenstates.

In both cases, the matrix elements of the Hamiltonian have to be set up. This does not pose a major challenge in case of small site numbers but in the general case it requires some clever way of creating and labeling of the Fock states, as described in a pedagogical way in [57].

[1] M. Greiner, O. Mandel, T. Esslinger, T. W. Hänsch, and I. Bloch, *Nature* **415** (2002).

[2] I. Bloch, J. Dalibard, and W. Zwerger, *Rev. Mod. Phys.* **80**, 885 (2008).

[3] A. Polkovnikov, K. Sengupta, A. Silva, and M. Vengalattore, *Rev. Mod. Phys.* **83**, 863 (2011).

[4] S. Trotzky, Y. Chen, A. Flesch, I. P. McCulloch, U. Schollwöck, J. Eisert, and I. Bloch, *Nat. Phys.* **8**, 325 (2012).

[5] D. Jaksch and P. Zoller, *Annals of Physics* **315**, 52 (2005), ISSN 0003-4916, special Issue.

[6] G. J. Milburn, J. Corney, E. M. Wright, and D. F. Walls, *Phys. Rev. A* **55**, 4318 (1997).

[7] S. Tomsovic, P. Schlagheck, D. Ullmo, J.-D. Urbina, and K. Richter, *Phys. Rev. A* **97**, 061606 (2018).

[8] C. Lee, T. J. Alexander, and Y. S. Kivshar, *Phys. Rev. Lett.* **97**, 180408 (2006).

[9] G. Arwas, A. Vardi, and D. Cohen, *Phys. Rev. A* **89**, 013601 (2014).

[10] K. Nemoto, C. A. Holmes, G. J. Milburn, and W. J. Munro, *Phys. Rev. A* **63**, 013604 (2000).

[11] R. Franzosi and V. Penna, *Phys. Rev. A* **65**, 013601 (2001).

[12] L. Simon and W. T. Strunz, *Phys. Rev. A* **89**, 052112 (2014).

[13] C. Khripkov, D. Cohen, and A. Vardi, *Phys. Rev. E* **87**, 012910 (2013).

[14] G. Santos, A. Tonel, A. Foerster, and J. Links, *Phys. Rev. A* **73**, 023609 (2006).

[15] J. Javanainen, *Phys. Rev. A* **81**, 051602(R) (2010).

[16] K. Furutani, J. Tempere, and L. Salasnich, *Phys. Rev. B* **105**, 134510 (2022).

[17] M. Chuchem, K. Smith-Mannschott, M. Hiller, T. Kottos, A. Vardi, and D. Cohen, *Phys. Rev. A* **82**, 053617 (2010).

[18] M. F. Herman and E. Kluk, *Chem. Phys.* **91**, 27 (1984).

[19] P. Schlagheck, D. Ullmo, G. M. Lando, and S. Tomsovic, *Phys. Rev. A* **106**, L051302 (2022).

[20] S. Ray, P. Ostmann, L. Simon, F. Grossmann, and W. T. Strunz, *J. Phys. A* **49**, 165303 (2016).

[21] S. Wüster, B. J. Dabrowska-Wüster, and M. J. Davis, *Phys. Rev. Lett.* **109**, 080401 (2012).

[22] S. Wimberger, G. Manganelli, A. Brollo, and L. Salasnich, *Phys. Rev. A* **103**, 023326 (2021).

[23] M. Albiez, R. Gati, J. Fölling, S. Hunsmann, M. Cristiani, and M. K. Oberthaler, *Phys. Rev. Lett.* **95**, 010402 (2005).

[24] A. J. Leggett, *Rev. Mod. Phys.* **73**, 307 (2001).

[25] F. T. Arecchi, E. Courtens, R. Gilmore, and H. Thomas, *Phys. Rev. A* **6**, 2211 (1972).

[26] M. Werther, S. Loho Choudhury, and F. Grossmann, *Int. Rev. in Phys. Chem.* **40**, 81 (2021).

[27] Y. Zhao, *J. Chem. Phys.* (2023).

[28] R. Hartmann, M. Werther, F. Grossmann, and W. T. Strunz, *J. Chem. Phys.* **150**, 234105 (2019).

[29] M. Werther and F. Grossmann, *Phys. Rev. A* **102**, 063710 (2020).

[30] E. J. Heller, in *Chaos and Quantum Physics*, edited by M. J. Giannoni, A. Voros, and J. Zinn-Justin (Elsevier, Amsterdam, 1991), Les Houches Session LII, pp. 547–663.

[31] Z. Huang, L. Wang, C. Wu, L. Chen, F. Grossmann, and Y. Zhao, *Phys. Chem. Chem. Phys.* **19**, 1655 (2017).

[32] A. Perelomov, *Generalized Coherent States and Their Applications* (Springer-Verlag, Berlin, 1986).

[33] W.-M. Zhang, D. H. Feng, and R. Gilmore, *Rev. Mod. Phys.* **62**, 867 (1990).

[34] F. Trimborn, D. Witthaut, and H. J. Korsch, *Phys. Rev. A* **77**, 043631 (2008).

[35] F. Trimborn, D. Witthaut, and H. J. Korsch, *Phys. Rev. A* **79**, 013608 (2009).

[36] J. Schachenmayer, A. J. Daley, and P. Zoller, *Phys. Rev. A* **83**, 043614 (2011).

[37] G. Mazzarella, L. Salasnich, A. Parola, and F. Toigo, *Phys. Rev. A* **83**, 053607 (2011).

[38] L. Dell'Anna, *Phys. Rev. A* **105**, 032412 (2022).

[39] P. Buonsante and V. Penna, *Journal of Physics A: Mathematical and Theoretical* **41**, 175301 (2008).

[40] Y. Qiao and F. Grossmann, *Phys. Rev. A* **103**, 042209 (2021).

[41] A. R. Kolovsky, *Journal of Modern Physics B* **30**, 1630009 (2016).

[42] P. Kramer and M. Saraceno, *Geometry of the time-dependent variational principle in quantum mechanics* (Springer Verlag, Berlin, 1981).

[43] A. Smerzi, S. Fantoni, S. Giovanazzi, and S. R. Shenoy, *Phys. Rev. Lett.* **79**, 4950 (1997).

[44] M. Göppert-Mayer, *Ann. Phys. (Leipzig)* **9**, 273 (1931).

[45] F. Grossmann, *Theoretical Femtosecond Physics: Atoms and Molecules in Strong Laser Fields* (Springer International Publishing AG, 2018), 3rd ed.

[46] E. M. Graefe and H. J. Korsch, *Phys. Rev. A* **76**, 032116 (2007).

[47] S. Wimberger, *Nonlinear Dynamics and Quantum Chaos: An Introduction* (Springer International Publishing AG, 2022), 2nd ed.

[48] S. Raghavan, A. Smerzi, S. Fantoni, and S. R. Shenoy, *Phys. Rev. A* **59**, 620 (1999).

[49] R. Gati and M. K. Oberthaler, *Journal of Physics B: Atomic, Molecular and Optical Physics* **40**, R61 (2007).

[50] M. Werther and F. Grossmann, *Phys. Rev. B* **101**, 174315 (2020).

[51] S. M. Barnett and D. T. Pegg, *J. Phys. A: Math. Gen.* **19**, 3849 (1986).

[52] S. Rau, J. Main, and G. Wunner, *Phys. Rev. A* **82**, 023610 (2010).

[53] O. E. Alon, A. I. Streltsov, and L. S. Cederbaum, *Phys. Rev. A* **77**, 033613 (2008).

[54] G. Dufour, T. Brüner, C. Dittel, G. Weihs, R. Keil, and A. Buchleitner, *New Journal of Physics* **19**, 125015 (2017).

[55] B. Gertjerenken and M. Holthaus, *Phys. Rev. A* **90**, 053622 (2014).

[56] E. M. Graefe, H. J. Korsch, and A. E. Niederle, *Phys. Rev. Lett.* **101**, 150408 (2008).

[57] J. M. Zhang and R. X. Dong, *European Journal of Physics* **31**, 591 (2010).